Taylor & Francis
Taylor & Francis Group

RESEARCH ARTICLE

Check for updates

The therapeutic prospect of zinc oxide nanoparticles in experimentally induced diabetic nephropathy

Samia A. Abd El-Baset [a], Nehad F. Mazen [a], Rehab S. Abdul-Maksoud [b], and Asmaa A. A. Kattaia [a]

aDepartment of Medical Histology and Cell Biology, Faculty of Medicine, Zagazig University, Zagazig Egypt; bDepartment of Medical Biochemistry, Faculty of Medicine, Zagazig University, Zagazig Egypt

ABSTRACT

Diabetic nephropathy (DN) is the most frequent cause of end-stage renal failure. Zinc oxide nanoparticles (ZnO-NPs) are promising antidiabetic agents. Our aim was to evaluate the prospective efficacy of ZnO-NPs in treating DN in streptozotocin-induced diabetic rats. Rats were randomly dispersed into three sets: control group, DN group and DN + ZnO-NPs group. ZnO-NPs were given at a dose of 10 mg/kg/day by oral gavage for 4 weeks. Urine and blood samples were processed for biochemical analyses. Kidney samples were managed for light and electron microscopy studies. Immune histochemical staining of P53, aquaporin11 (AQP11) and mechanistic target of rapamycin (mTOR) were performed. Gene analyses of nephrin, podocin, beclin-1, LC3 and p62 were done. Administration of ZnO-NPs ameliorated the functional and histopathological alterations of the kidney in a rat model of diabetic nephropathy. ZnO-NPs retained the constancy of the glomerular filtration barrier and restored almost normal renal structure. This was confirmed by upregulation of mRNA expression of podocyte markers (nephrin and podocin) and AQP11 immune histochemical expression in the renal tubules. The beneficial outcomes of ZnO-NPs might be attributed to activation of autophagy through inhibiting mTOR signaling pathway. ZnO-NPs enhanced beclin-1 and LC3 mRNA expressions and reduced p62 mRNA expression. ZnO-NPs also exerted anti-apoptotic potential (evidenced by the decrease in p53 immune expression), anti-inflammatory and anti-oxidant effect [endorsed by suppression of serum cyclooxygenase-2 (COX-2) enzyme activity, tissue nuclear factor kappa beta (NF-κB) level and blood hypoxia-inducible factors (HIF-1α) level]. These results may point the way to an effective therapy of DN.

Abbreviations: AQP11 Aquaporin11; BUN: Blood urea nitrogen; COX-2: Cyclooxygenase-2; DAB: 3, 3'-diaminobenzidine; DM: Diabetes mellitus; DN: Diabetic nephropathy; ELISA: Enzyme-linked immunosorbent assay; H&E: Hematoxylin & eosin; HIF-1α: Hypoxia-inducible factors; iNOS: inducible nitric oxide synthase; LC3: Microtubule-associated protein 1 light chain 3; mTOR: Mechanistic target of rapamycin; NF-κB: Nuclear factor kappa beta; NPs: Nanoparticles; PAS: Periodic acid Schiff; PCR: Polymerase chain reaction; PGE2: Prostaglandin E2; ROS: Reactive oxygen species; STZ: Streptozotocin; X ± SEM: Mean ± standard error of means; Zn: Zinc; ZnO-NPs: Zinc oxide nanoparticles.

Introduction

Diabetes mellitus (DM) is a major health problem resulting in about 1.5 million deaths per year all over the world.[1] A major complication of DM is diabetic nephropathy (DN), which accounts for half of the end-stage kidney disease.[2]

Pathological changes occurring in the kidney and resulting in diabetic nephropathy are multifactorial. Hyperglycemia induces podocyte injury and decreases their number leading to rapid decline in the glomerular filtration barrier function and eventually renal function deterioration.[3,4] The glomerular filtration membrane and podocyte function are maintained through two proteins. nephrin and podocin.[5] Changes in these protein expressions play a major role in DM-induced proteinuria and deteriorated renal function.[6]

Additionally, hyperglycemia causes further increase in tubular reabsorption of glucose and sodium causing activation of sodium-potassium-ATPase leading to enhancement of oxygen consumption with hypoxia of the proximal tubules.[7,8] Both tissue hypoxia and hyperglycemia induce activation of hypoxia-inducible

CONTACT Asmaa A. A. Kattaia ✉ asmaaalhosiny7@gmail.com; ehabmohomar@yahoo.com; AAKataya@medicine.zu.edu.eg 🏢 Faculty of Medicine, Zagazig University, Zagazig, Asharquia, Egypt, Postal code: 44519

factors (HIF-1α), which in role promotes tubulointerstitial fibrosis and plays a key role in glomerular damage.[9]

At the level of renal tubules and defective water channel proteins, aquaporins (AQPs) expression may be responsible for polyuria in DM,[10] and predispose to hyperglycemia-induced fibrosis, oxidative stress and further tubular dysfunction.[11] Hyperglycemia is also associated with activation of nuclear factor kappa beta (NF-κB) with subsequent induction of proximal tubular cyclooxygenase-2 (COX-2) leading to increased prostaglandin E2 (PGE2) production and protein excretion[12,13].

Although oxidative stress is an important factor during pathogenesis of DN,[14] other pathways are also involved in autophagy.[15] Hyperglycemia induced impaired podocyte autophagic activity through activation of mechanistic target of rapamycin (mTOR).[16] mTOR is encoded by mTOR gene and related to the phosphatidylinositol kinase family proteins. It controls metabolism, growth and survival of the cells, and is regulated by hormones, growth factors and stressful conditions.[17] In the same context, beclin-1 is an essential element in activating autophagy. It becomes a part of the autophagosome membrane and promotes autophagy nucleation.[18] Microtubule-associated protein 1 light chain 3 (LC3) is a ubiquitin-like protein that is involved in autophagy. LC3 is cut to liberate the cytosolic LC3-I, which is transformed to the membrane-bound LC3-II that is then incorporated into autophagosomes. The increase of LC3-II signifies the number of autophagosomes.[19] LC3 buildup is either due to enhanced autophagosome formation or decreased autophagosome-lysosome fusion. To differentiate between the two probabilities, p62 could be examined, its accumulation indicates blockage of autophagosome clearance. P62 protein acts as a receptor for ubiquitinated proteins, binds LC3-II followed by degradation in autolysosomes.[20]

Zinc (Zn) is a trace element involved in the structure of different enzymes in the human body[21] and participates in several metabolic processes including glucose metabolism.[22] It plays a fundamental role in insulin formation and secretion.[23] Zn imbalance may be considered as one of the contributing factors of DM.[24] Zn is a promising therapeutic agent in DM, but its poor bioavailability may hinder its usage.[25]

In spite of recent advances to manage DN, effective strategies to prevent disease progression to end-stage renal failure are lacking. Nanomaterials were widely explored to reveal their possible effectiveness in the management of several diseases. Due to their special chemical and physical characteristics, ZnO-NPs have been extensively used as potential therapeutic agents. ZnO-NPs are also effective agents in Zn delivery owing to their small size and good bioavailability.[26]

Accordingly, this study aims to explore the prospective efficacy of ZnO-NPs in ameliorating DN through assessing different signaling pathways in streptozotocin-induced diabetic rats.

Materials and methods

Chemicals

Streptozotocin (STZ; CAS No. 18883–66-4; Sigma–Aldrich, Saint Louis, USA) is a powder of 95% purity.

Zinc oxide nanoparticles (ZnO-NPs) are obtained from Sigma–Aldrich (CAS No. 1314–13-2; Saint Louis, USA). They are in the form of a dispersion with a concentration of 50% wt. in H_2O, a pH of 7 ± 0.1, a hydrodynamic diameter of <100 nm (average particle size 40 nm) based on the dynamic light scattering method, a density of 1.7 ± 0.1 g/mL at 25°C and a zeta potential of -33.20 ± 3.56 mV, as specified by the supplier.

Experimental animals

Thirty-five (6 to 7 weeks old) male albino rats weigh 180–200 g. They were purchased from the Breeding Animal House, Faculty of Medicine, Zagazig University, Egypt. Plastic cages with wire mesh tops housed rats. They were placed in a room with a controlled temperature 25–27°C, a regular cycle of light/dark of 12/12 hours and a humidity range of 40–

70%. A standard rat chow was used to feed animals with free accession to clean water. Rats were acclimatized for 1 week.

Ethics approval

All applicable international and institutional guidelines for the care and use of animals were followed. The animal procedures were approved by Institutional Animal Care and Use Committee IACUC (protocol approval number: 5824), Zagazig University, Egypt.

Characterization of ZnO-NPs

The shape and size of ZnO-NPs were examined by JEOL JEM 2100 transmission electron microscopy (Jeol Ltd, Tokyo, Japan). Dropping of the aqueous dispersion of NPs was done on a carbon-coated copper grid that was dried and then inspected.

Induction of experimental diabetic nephropathy (DN)

Type I diabetes was provoked by a single intraperitoneal injection of STZ (50 mg/kg) in overnight fasted rats. Ten minutes before injection, STZ was freshly liquefied in cold citrate buffer (0.1 M, pH4.5). After the injection, rats were given sucrose (15 g/L) in the drinking water for 24 hours to decrease death from the probable hypoglycemic shock. Diabetes was confirmed by testing fasting blood glucose level, 3 days following STZ injection. Fasting blood glucose concentrations surpassing 250 mg/dL were considered diabetic, and rats were included in the experiment. DN was evaluated after 6 weeks by measuring serum creatinine, blood urea nitrogen (BUN) and proteins in urine.[27] Rats with high levels were incorporated in the study. Three rat models of DN died and two rats were excluded. Treatment with ZnO-NPs was started 6 weeks following STZ injection.

Study design

Rats were randomly dispersed into three sets. Group I (control group, $n = 10$) was received an intraperitoneal injection of 0.5 mL citrate buffer (vehicle of STZ, 0.1 M, 4.5pH), group. Rat models (20 rats) were equally subdivided into two groups; group II (DN group) and group III (DN + ZnO-NPs group), which were treated with ZnO-NPs at a dose of 10 mg/kg/day by oral gavage for 4 weeks.[28] The chosen dose of ZnO-NPs was 1/50 of LD50. The LD50 of ZnO-NPs was determined as ≥500 mg/kg/day for rats.[29]

Sampling

Sampling of blood and urine was performed at the end of 6th and 10th weeks. For urine samples collection, over a 24-h period and within metabolic cages, urine samples were collected in protease inhibitor containing glass bottles. Urine samples were purified by centrifugation at $3000 \times g$ for 10 min and stored at −20°C until analysis. For blood samples collection, blood was taken from the retro-orbital veins, and collected in either plain tubes (for serum preparation) or EDTA containing tubes.

After 10 weeks from the start of the experiment, the rats were euthanized by intraperitoneal injection of 50 mg/kg sodium phenobarbital.[30] Both kidneys were excised and processed for biochemical and histopathological examinations

Tissue preparation for biochemical analysis

By using a homogenizer (Janke and Kunkel, Germany), weighed kidney samples were homogenized into 10 parts (w/v) of 50 mM Tris-HCl (pH 7.4). Centrifugation of the homogenate was performed for 15 minutes at 3,000 rpm and the supernatant was collected for further analysis.

Biochemical investigations

Estimation of total protein in urine

The concentration of total proteins was determined calorimetrically in the 24-hr urine samples using a commercially available kit provided by SPINREACT (Sant Esteve de Bas, Spain) according to the manufacturer's protocol.

Blood glucose

Its level was estimated using glucose estimation kit [SPINREACT, Sant Esteva de Bas, Spain) depending on the method of [31].

Serum insulin

Its determination was achieved using enzyme-linked immunosorbent assay (ELISA] kit (Cayman Chemical, Ann Arbor, MI).

Serum creatinine and blood urea nitrogen (BUN)

Their estimations were accomplished using commercially available kits according to the guidelines of the manufacturers (ACCUREX, Biomedical Pvt. Ltd).

Hypoxia inducible factor-1 alpha (HIF-1α)

It was assayed in rat blood by HIF-1α ELISA kit (BioVision, Inc. Milpitas, CA) depending on the manufacturer's manual.

Cyclooxygenase-2 (COX-2) enzyme

Its activity *was* measured in the serum using a COX activity assay kit (Cayman Chemical, Ann Arbor, MI).

Nuclear factor kappa beta (NF-κB)

It was measured in kidney tissue homogenates by using ELISA kit (Cayman Chemical, Ann Arbor, MI).

Analysis of nephrin, podocin, beclin-1, LC3 and p62 genes

Isolation of RNA and reverse transcription

Renal tissue total RNA was extracted using TRIzol reagent (Invitrogen; Thermo Fisher Scientific, Inc.). Reverse transcription of the extracted RNA to complementary DNA (cDNA) was performed using First-Strand cDNA Synthesis kit (Life Technologies, USA) according to the instruction manual.

Real time polymerase chain reaction (real-time PCR)

Real-time PCR was performed using SuperReal PreMix Plus (SYBR Green PCR master mix; Tiangen Biotech Co., Ltd.) on the ABI 7500 (Applied Biosystems, Foster, CA). GAPDH was used as internal control for data normalization. The following primers were used: nephrin forward, 5'-CAACTGGGAGAGACTGGGAGAA-3', reverse, 5'-AATCTGAAACAAGACGGAGCA-3'; podocin forward, 5'-AAGAGTAATTATATTCCGACTGGGACAT-3', reverse, 5'-TGGTCACGATCTCATGAAAAGG-3'; beclin-1 forward, 5'-TTGGCCAATAAGATGGGT CTGAA-3', reverse, 5'-TGTCAGGGACTCCAG ATACGAGTG-3'; LC3 forward, 5'-CATGCCG TCCGAGAAGACCT-3'; reverse, 5'-GATGAGC CGGACATCTTCCACT-3'; p62 forward, 5'-GCCCTGTACCCACATCTCC-3'; reverse, 5'-CCATGGACAGCATCTGAGAG-3'; GAPDH forward, 5'-TGCCACTCAGAAGACTGTGG-3'; reverse, 5'-GGATGCAGGG-ATGATGTTCT-3'.

The following thermal conditions were used: for beclin-1, LC3 and p62, denaturation at 94°C for 10 min, then 40 cycles at 94°C for 15 sec, 58°C for 30 s and finally at 72°C for 40 s; for nephrin and podocin, initial hot start at 95°C for 15 min, then 45 cycles for 15 s at 94 °C, 30 s at 56°C, and 30 s at 72°C. The reactions were performed in triplicate. PCR reaction mixture was as follow: 12.5 μl 2× SuperReal PreMix Plus, 0.75 μl of each primer, 2 μl cDNA template, RNase-free ddH$_2$O up to a final volume of 25 μl. Gene expression levels were calculated according to the $2^{-\Delta\Delta CT}$ method.[32]

Light microscope study

Specimens were mounted in buffered formalin (10%) and processed to prepare paraffin sections (5–7 μm thick) for staining with hematoxylin & eosin (H&E), Mallory's trichrome, Periodic acid Schiff (PAS), and immune histochemical stains.[33] For immune histochemistry, the method of avidin biotin complex (Thermo Scientific, USA, Cas No. 32020) was used following the manufacturer's guidelines. The primary antibodies of p53 (rabbit polyclonal antibody, catalog #: ab131442, at 1/50 dilution; Abcam, Cambridge, USA), aquaporin11 (AQP11) (rabbit polyclonal antibody, catalog #: NBP1-86208, at 1/20 dilution; Novus Biologicals, USA), Mechanistic target of rapamycin (mTOR) (rabbit polyclonal antibody, catalog #: MBS9610665, at 1/20 dilution, MyBioSource, Inc., USA) were obtained. Biotinylated secondary

antibodies with labeled horseradish peroxidase, then 3, 3'-diaminobenzidine (DAB) staining allowed to detect brown positive reactions. The counterstain Mayer's hematoxylin was used. To get negative controls, the primary antibodies were excluded.

Electron microscopy study

Specimens were instantly fixed in phosphate-buffered glutaraldehyde (2.5%, pH 7.4), followed by osmium tetroxide (1%) at 4°C in the same buffer, next dehydrated and embedded in epoxy resin. Ultrathin sections (50 nm in thickness) were obtained using Leica ultra-cut UCT, then stained with uranyl acetate and lead citrate.[34] Photography was achieved by JEOL JEM 2100 transmission electron microscopy (Jeol Ltd, Tokyo, Japan) in Electron Microscopy Research Laboratory, Faculty of Agriculture, El Mansoura University, Egypt.

Morphometric study

For morphometric analysis, we used FIJI image processing software, a distribution of ImageJ2 (open source; GNU General Public License). The measurements were managed by an unaware examiner to the experiment. Measurements were accomplished in five images taken at 400× magnification in five non-overlapping random fields per rat in each group.

Area percentage (%) of collagen fibers in Mallory's trichrome-stained sections, positive reactions in PAS-stained sections and positive immunoreactions in anti-AQP11 and anti-mTOR immune-stained sections were measured. The count of brown cells in anti-p53 immune-stained sections was also evaluated.

Statistical analysis

Statistical Package for Social Sciences (SPSS, version 22.0, IBM Corp, NY, USA) was utilized for analysis. All data were expressed as mean ± standard error of means ($X \pm SEM$). To compare the means, a one-way analysis of variance (ANOVA)
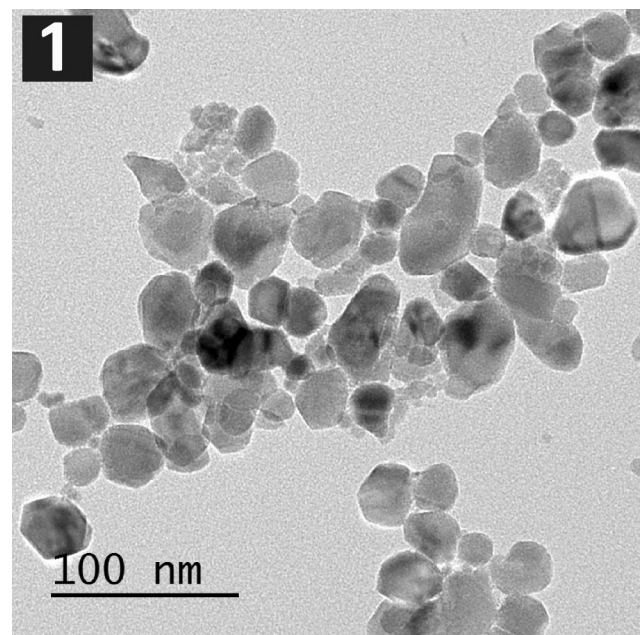
Figure 1. Transmission electron microscopy image showing average diameters of ZnO-NPs.

was applied, afterword the post-hoc test; Tukey's HSD test. P values were regarded significant when <0.05 and highly significant when <0.001.

Results

Characterization of ZnO-NPs

They appeared mostly spherical with diameters <100 nm (the average particle size 40 nm) (Figure 1).

Biochemical results

Measurements of blood glucose, blood urea nitrogen (BUN), serum creatinine and urinary protein excretion in DN group at the end of 6th and 10th weeks showed highly significant increases ($p< .001$), while serum insulin exhibited a highly significant decrease ($p< .001$) when compared to the control group. On the contrary, treatment with ZnO-NPs by the end of the 10th week revealed highly significant reductions in blood glucose, BUN, serum creatinine and urinary protein levels and a highly significant enhancement in serum insulin level ($p< .001$), compared to the DN group (Figure 2).

There were highly significant rises in blood HIF-1α, serum COX-2 enzyme activity and NF-κB in the renal tissues of DN group ($p < .001$), compared to the normal controls. Conversely, DN + ZnO-NPs group displayed highly significant decreases regarding the former parameters ($p < .001$) in comparison to the DN group (Table 1).

Real-time polymerase-chain reaction (PCR) gene expression results
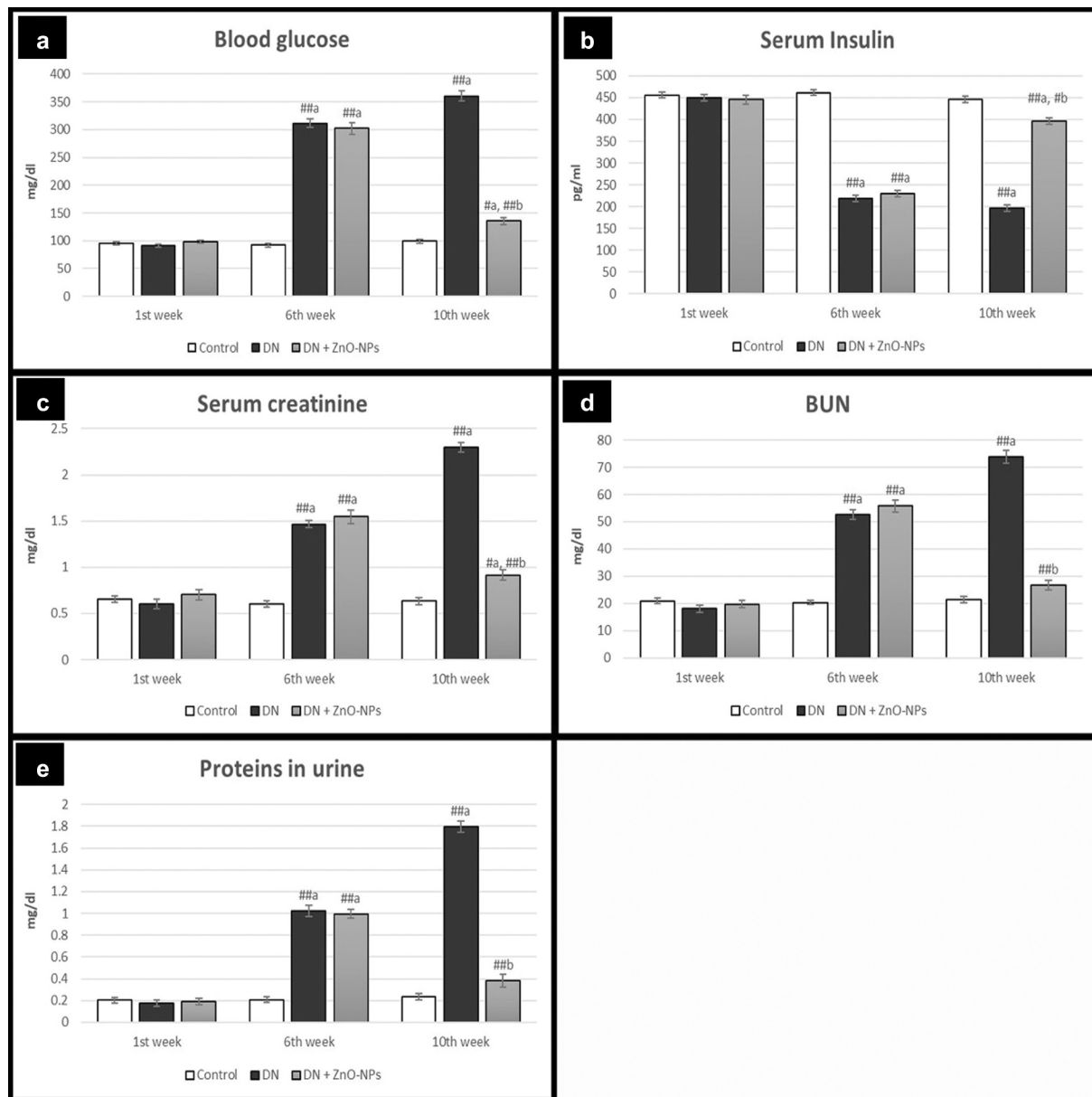
Figure 2. Measurements of biochemical parameters; BUN, blood urea nitrogen; Values are displayed as mean ± standard errors ($X \pm SEM$); [a]: P compared to control group; [b]: P compared to DN group; [#]: $P < .05$; [##]: $P < .001$; $n = 10$.

Table 1. Measurements of oxidative stress and inflammatory parameters.

	Control group	DN group	DN + ZnO-NPs group
HIF-1α (ng/ml)	0.36 ± 0.06	2.13 ± 0.2[##a]	0.66 ± 0.08[##b]
COX-2 (U/ml)	7.52 ± 0.51	35.42 ± 1.3[##a]	12.36 ± 0.77[#a, ##b]
NF-κB (pg/mg protein)	0.14 ± 0.03	1.08 ± 0.11[##a]	0.23 ± 0.04[##b]

HIF-1α, hypoxia inducible factor-1 alpha; COX-2, cyclooxygenase-2; NF-κB, nuclear factor kappa beta. Values are displayed as mean ± standard error (X ± SE); [a]: P compared to control group; [b]: P compared to DN group; [#]: $P < 0.05$; [##]: $P < 0.001$; n = 10.

DN group showed highly significant down-regulation concerning nephrin, podocin, beclin-1 and LC3 mRNA levels ($p< .001$) and highly significant upregulation in p62 ($p< .001$), compared to the controls. DN + ZnO-NPs group revealed significant increases in nephrin and podocin ($p< .05$), highly significant increases in beclin-1 and LC3 gene expressions ($p< .001$) and a highly significant decrease in p62 ($p< .001$) compared to DN group. On the other hand, the differences weren't significant regarding nephrin, LC3 and p62 mRNA expressions ($p> .05$) in comparison with the control group (Figure 3).

Histopathological results

H&E stain results

Examination of H&E-stained sections in adult male rats' renal cortex of the control group showed that the glomeruli appeared normal, Bowman's capsule
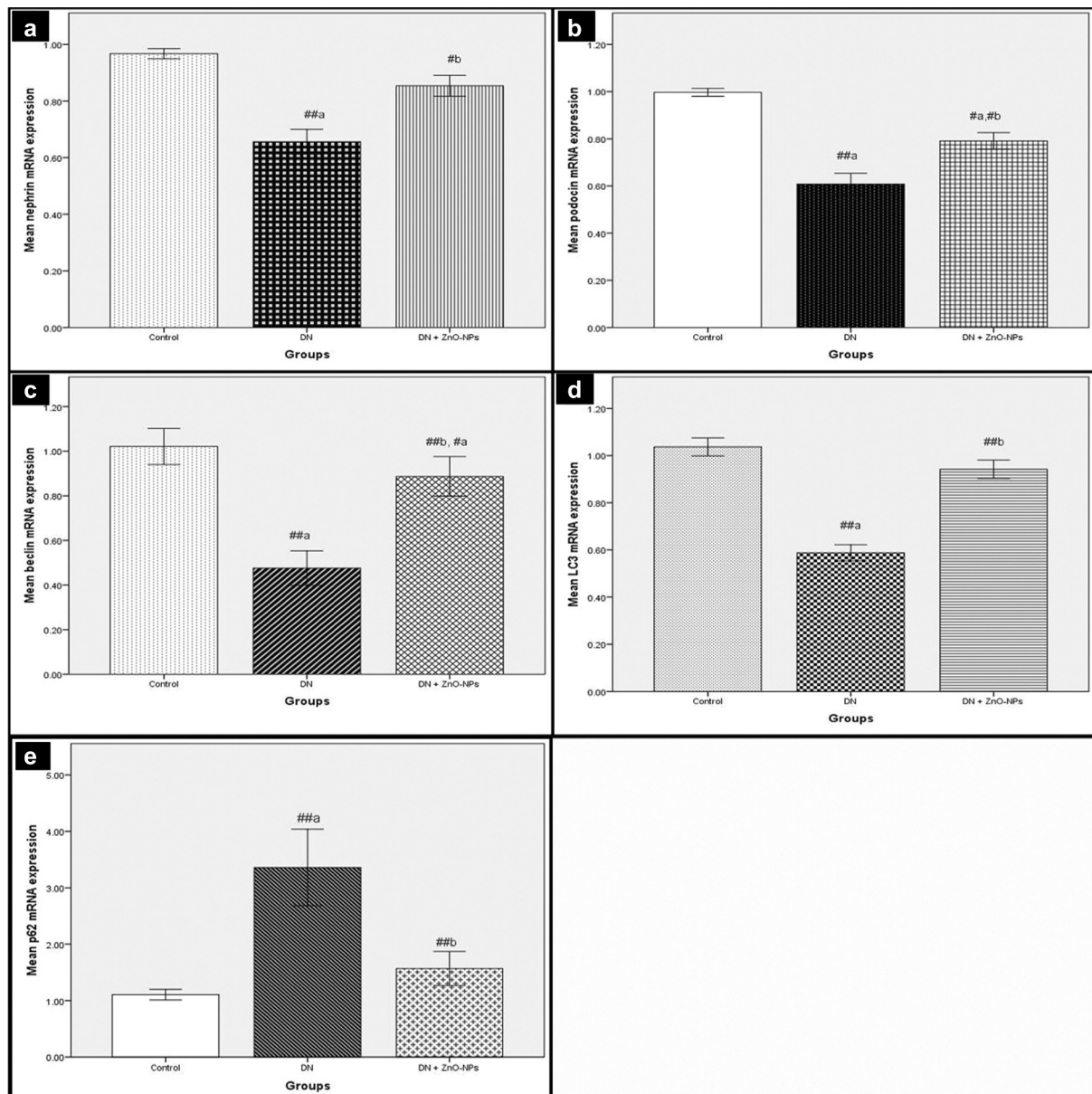

Figure 3. Real-time PCR analyses of mRNA levels of nephrin, podocin, beclin-1, LC3 and p62 in the renal cortex. Values are displayed as mean ± standard errors ($X ± SEM$); [a]: P compared to control group; [b]: P compared to DN group; [#]: $P< .05$; [##]: $P< .001$; $n = 10$.

were lined by simple squamous cells with normal Bowman's space. Normal proximal and distal convoluted tubules were seen (Figure 4a).

Examination of DN group sections showed some glomeruli with mesangial expansion, some appeared segmented with mesangial expansion and narrow Bowman's space, and others had thickened parietal layer of Bowman's capsule. The tubules had vacuolated lining cells, hyaline and cellular casts within their lumen. The interstitial spaces showed infiltrating mononuclear inflammatory cells, dilated congested blood vessels and others with thickened wall, extravasated red blood cells, exudate and increased fibrous tissue (Figure 4b-e).
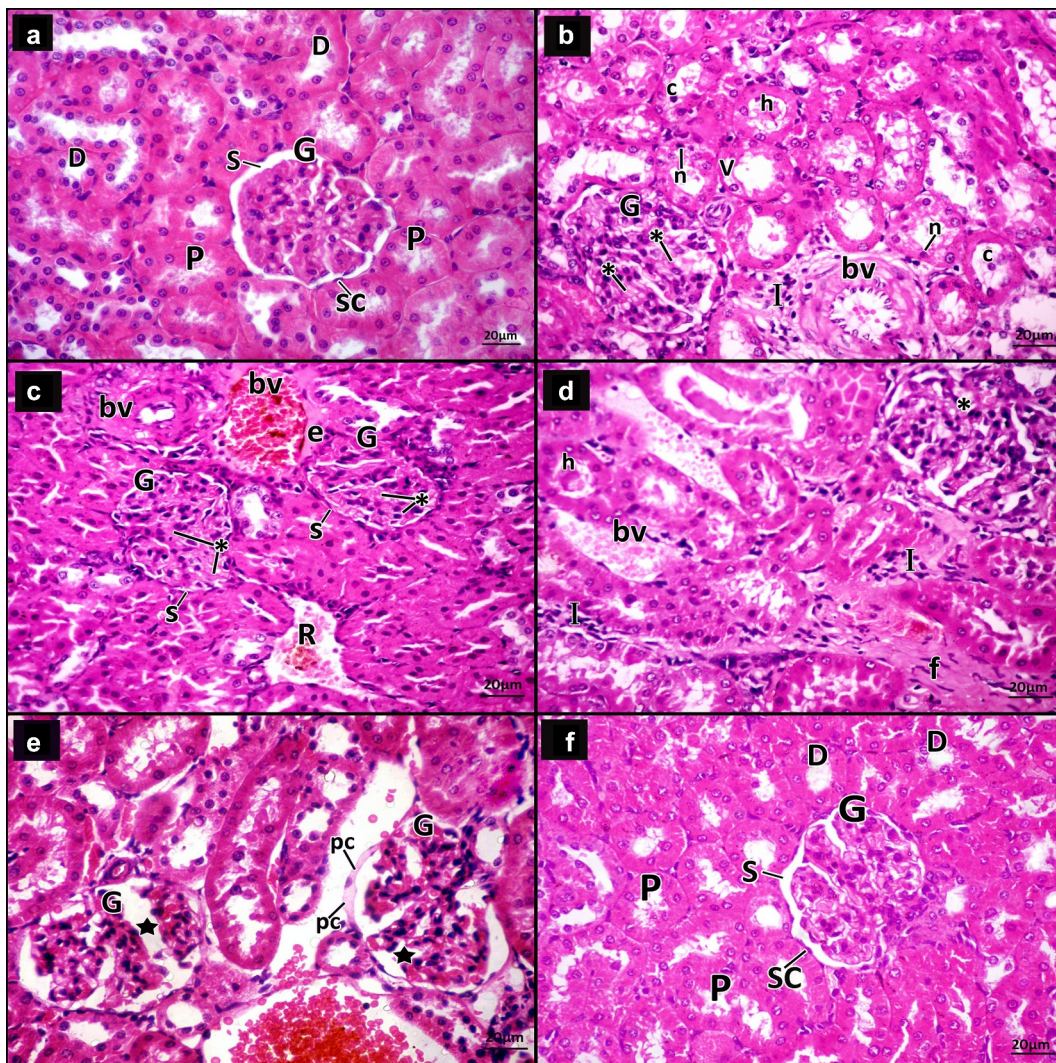
Figure 4. A photomicrograph for H&E-stained sections in adult male rats' renal cortex. **a** Control group, the glomerulus (g) appears normal, Bowman's capsule is lined by simple squamous cells (SC) and Bowman's space (s) appears narrow. Proximal (p) and distal convoluted tubules (d) are seen. **b–e** DN group. **b** The glomerulus (G) shows mesangial expansion (*). Some tubules have vacuolated lining cells (v), small dark nuclei (n) and hyaline (h) and cellular (c) casts within their lumen. The interstitium shows infiltrating mononuclear inflammatory cells (i) and thickened blood vessels (bv). **c** The glomeruli (G) show mesangial expansion (*) and narrow Bowman's space (s). The interstitium shows congested blood vessel (bv) surrounded by an exudate (e), a blood vessel with thickened wall (bv) and extravasated red blood cells (r). **d** The glomeruli (G) appear segmented with mesangial expansion (*). The tubules have hyaline (h) casts within their lumen. The interstitium shows infiltrating mononuclear inflammatory cells (I), dilated congested blood vessels (bv) and increased fibrous tissue (f). **e** The glomeruli (G) appear segmented (star) with swollen parietal layer of Bowman's capsule (pc). Notice dilated congested blood vessel within the interstitium (bv). **f** DN + ZnO-NPs, the glomeruli (G) appear almost normal, Bowman's capsule is lined by simple squamous cells (SC) and the Bowman's space (s) is about normal. Nearly normal proximal (P) and distal convoluted tubules (D) are seen.

DN + ZnO-NPs group sections showed almost normal glomeruli, Bowman's capsule was lined by simple squamous cells and normal Bowman's space. Nearly normal proximal and distal convoluted tubules were seen (figure 4f).

Mallory's trichrome stain results

Light microscopy examination of Mallory's trichrome-stained sections of the renal cortex of the controls revealed a few collagen fibers (Figure 5a). Diabetic group sections showed increased collagen fibers around renal tubules and renal corpuscles, in between glomerular capillaries and within and around the wall of the blood vessels (Figure 5b). Sections of DN + ZnO-NPs group showed almost normal distribution of collagen fibers (Figure 5c).

PAS results

Examination of PAS-stained sections of the renal cortex of the control group showed normal reaction in the basement membrane of tubular epithelium and glomerular capillaries, along with the parietal epithelial cells of Bowman's space. The reaction also appeared at the brush border of the renal tubules (Figure 6a). Diabetic group sections revealed increased reaction in the basement membrane of tubular epithelium, glomerular capillaries and along with the parietal epithelial cells of Bowman's space, in addition to the increased mesangium. The reaction was also increased at the brush borders of the renal tubules (Figure 6b). DN + ZnO-NPs group sections showed a nearly normal reaction comparable to the controls (Figure 6c).
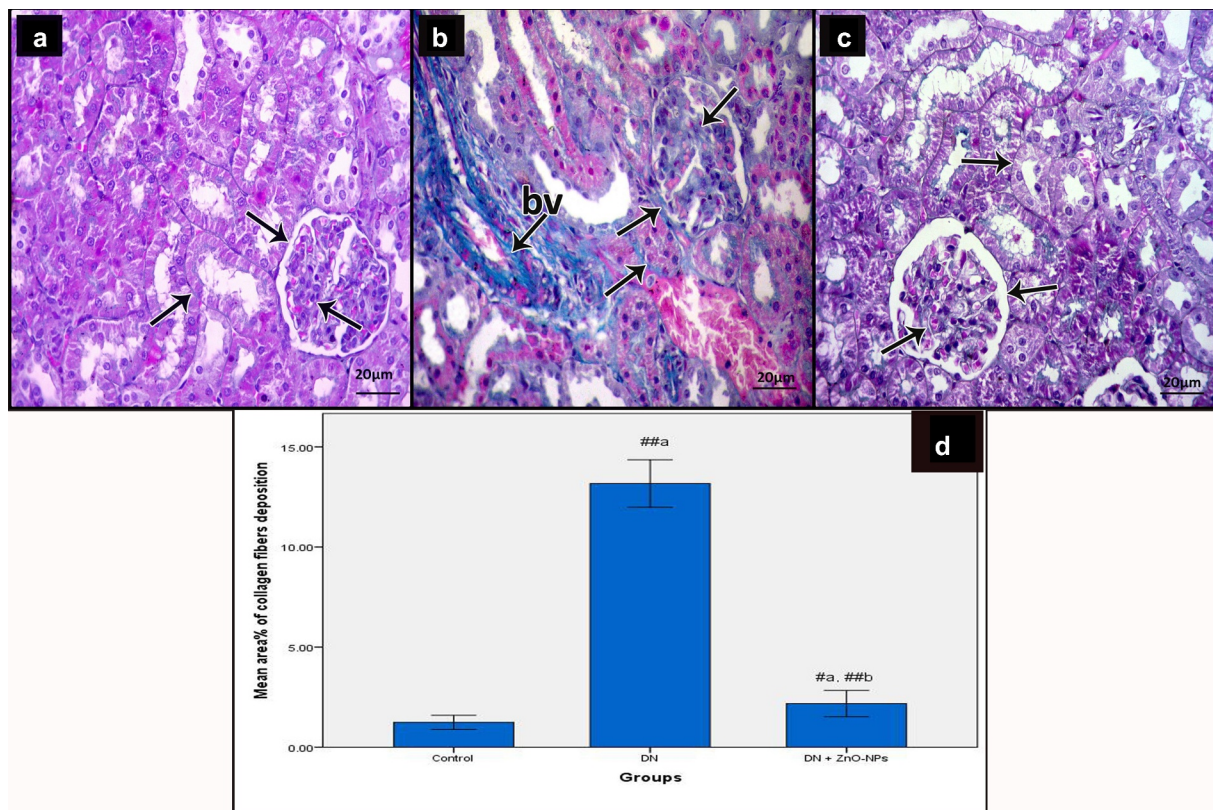
Figure 5. Mallory's trichrome stained sections of the renal cortex of the study groups. Collagen fibers (arrow) **a** Control group, showing few collagen fibers. **b** DN group, showing increased collagen fibers around renal tubules and renal corpuscles, in between glomerular capillaries and within and around the wall of the blood vessels (bv). **c** DN + ZnO-NPs, showing nearly normal distribution of collagen fibers. **d** The mean area % of collagen fibers in Mallory's trichrome-stained sections. Values are displayed as mean ± standard errors ($X \pm$ SEM); [a]: P compared to control group; [b]: P compared to DN group; [#]: $P <$ .05; [##]: $P <$ .001.

Immune histochemical results

Immune localization of p53 of the control group sections showed nuclear reaction in few cells (Figure 7a). In the diabetic group, the reaction appeared in many cells' nuclei (Figure 7b). DN + ZnO-NPs group revealed nuclear reaction in some cells (Figure 7c).

Examination of sections stained with AQP11 in the control group revealed intense cytoplasmic reaction in most of the tubular cells (Figure 8a). Diabetic group sections showed some tubular cells with faint reaction (Figure 8b). In DN + ZnO-NPs group, cytoplasmic reaction could be detected in many tubular cells (Figure 8c).

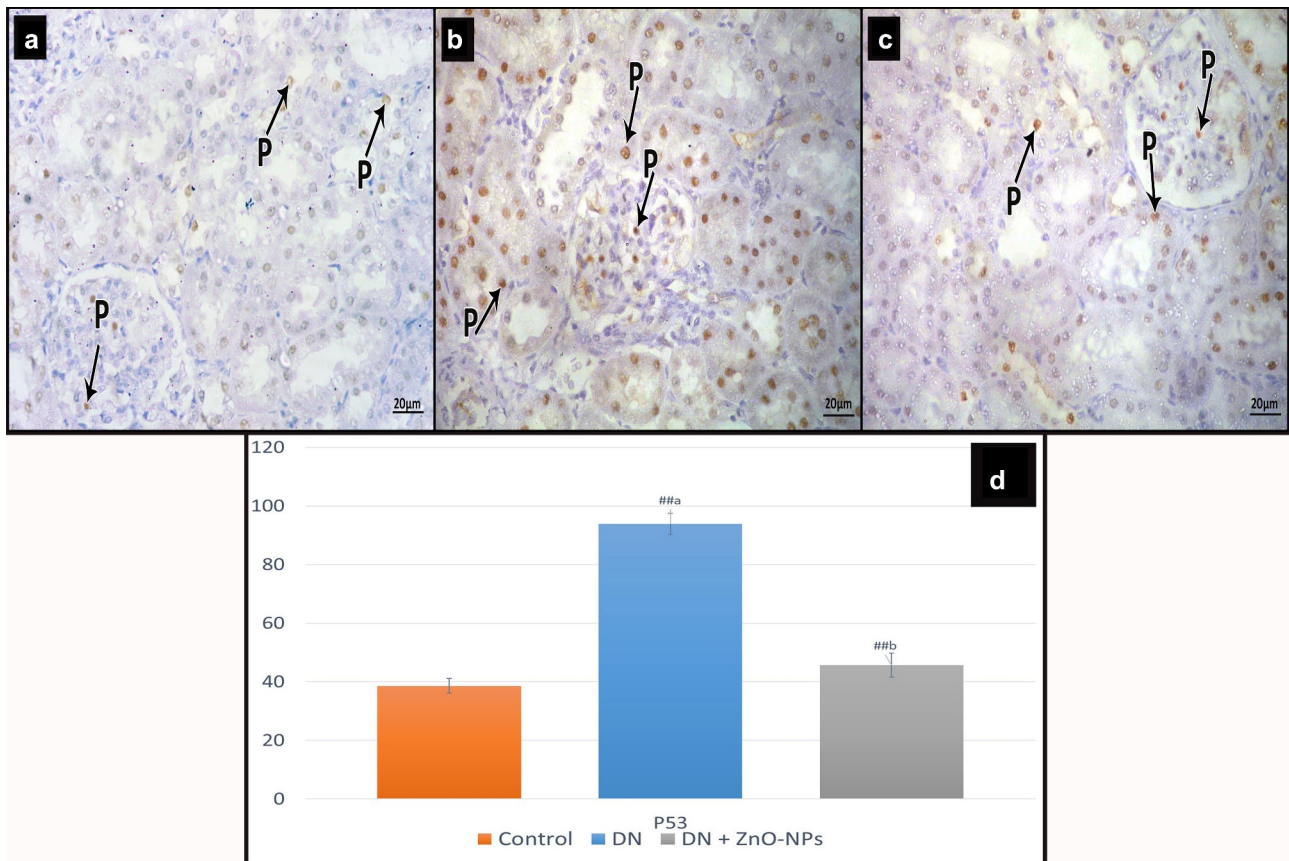Immune-stained sections for mTOR in the control group showed few immune reactive cells (Figure 9a). Examination of diabetic group sections revealed positive reaction (cytoplasmic or nuclear) in many tubular and glomerular cells (Figure 9b). Sections of DN + ZnO-NPs group showed some immune reactive cells (Figure 9c).

Ultrastructure results

Ultrathin sections examination of the glomeruli of the control group showed primary processes arising from of glomerular podocytes. The filtration barrier was formed of many thin foot processes, basement membrane and fenestrated endothelium of the glomerular capillaries with red blood cells in their lumen (Figure 10a). Proximal tubular cells appeared resting on a thin regular basement membrane. They had regular euchromatic nuclei with prominent
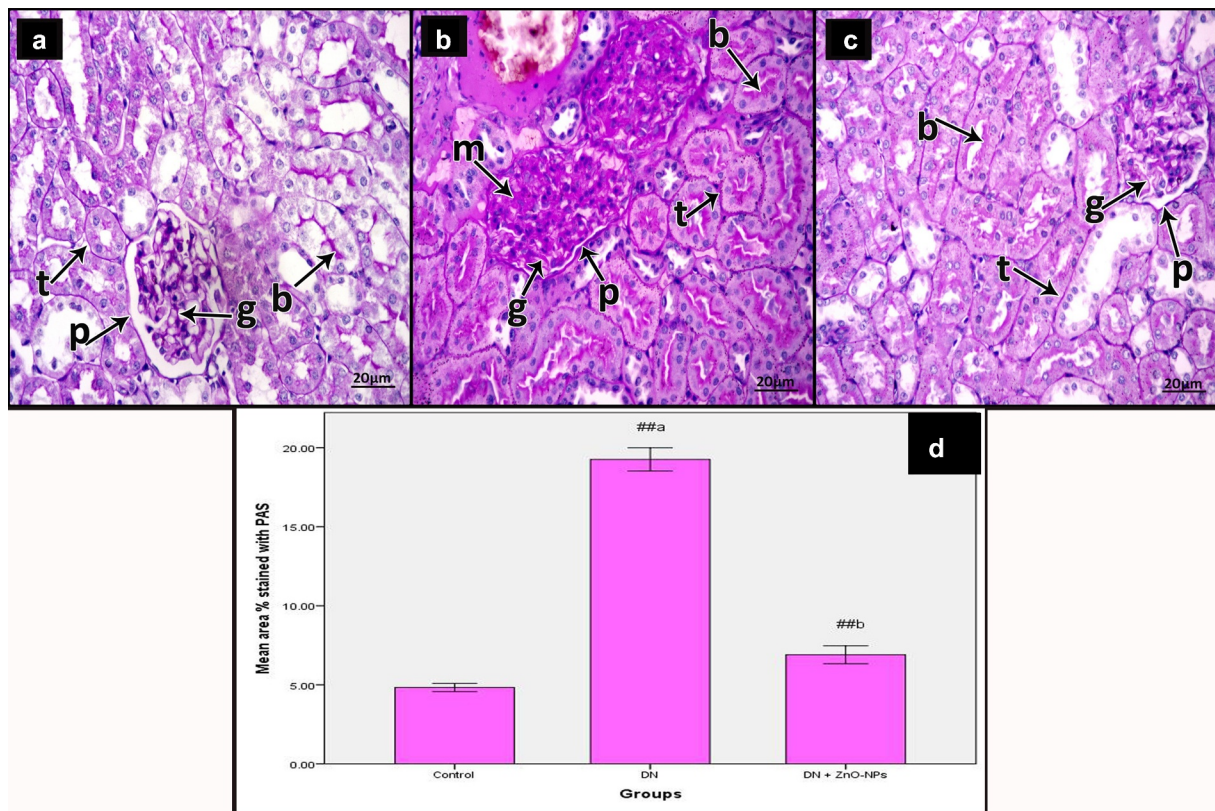
Figure 6. Periodic acid Schiff-stained sections of the renal cortex of the study groups. **a** Control group, showing reaction in the basement membrane (arrow) of tubular epithelium (t), glomerular capillaries (g) and along with the parietal epithelial cells of Bowman's space (p). The reaction also appears in the brush borders of the renal tubules (b). **b** DN group, showing increased reaction in the basement membrane (arrow) of tubular epithelium (t), glomerular capillaries (g) and along with the parietal epithelial cells of Bowman's space (p) in addition to increased mesangium (m). The reaction is increased in the brush borders of the renal tubules (b). **c** DN + ZnO-NPs, showing nearly normal reaction in the basement membrane (arrow) of tubular epithelium (t), glomerular capillaries (g) and along with the parietal epithelial cells of Bowman's space (p). The reaction also appears in the brush borders of the renal tubules (b). **d** The mean area % of positive reactions in PAS-stained sections, values are displayed as mean ± standard errors ($X \pm$ SEM); [a]: P compared to control group; [b]: P compared to DN group; [#]: $P < .05$; [##]: $P < .001$.
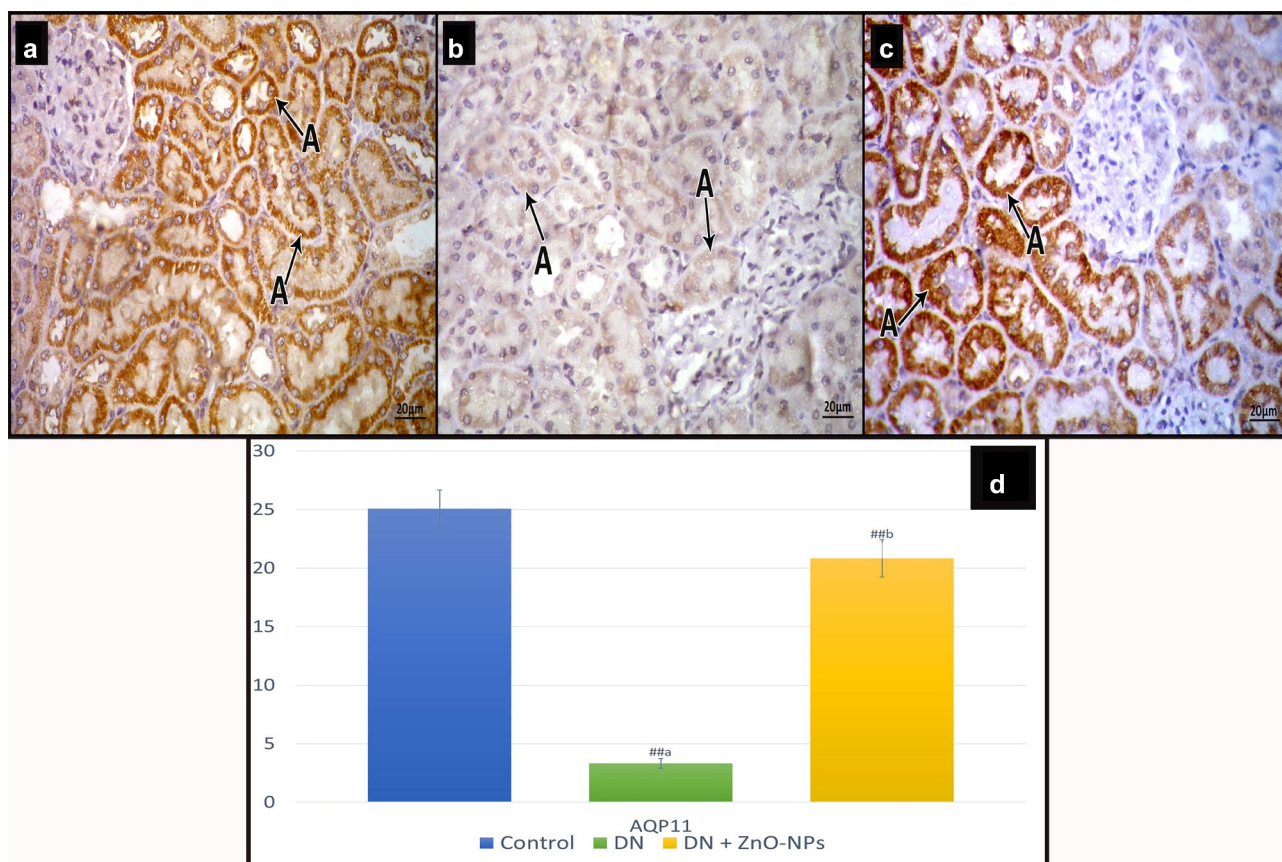
Figure 7. Immune histochemical-stained sections for P53 in the renal cortex of albino rats in the study groups. P53 nuclear immune reactions (p). **a** Control group, reaction appears in few cells. **b** DN group, showing the reaction in many cells. **c** DN + ZnO-NPs groups, showing the reaction in some cells. **d** The average count of brown nuclei in anti-p53 immune-stained sections. Estimates are displayed as mean ± standard errors (X ± SEM); [a]: P compared to control group; [b]: P compared to DN group; [#]: $P< .05$; [##]: $P< .001$.

nucleoli and regularly packed apical microvilli. The basal part showed basal infoldings with regularly arranged mitochondria (Figure 11a). The collecting tubular cells had regular euchromatic nuclei with prominent nucleoli. They had smooth apical membrane away from few short microvilli and numerous mitochondria. The cells were attached to each other by tight junction (Figure 12a).

Diabetic group sections revealed disrupted filtration barrier; the podocyte foot processes showed effacement, some areas of the glomerular basement membrane appeared thick and the glomerular capillaries showed disappearance of fenestrated endothelium in some areas (Figure 10b). The proximal tubular cells rested on a thick basement membrane. The tubular cells had heterochromatic nuclei, rarified cytoplasm with some vacuolated areas and disorganized apical microvilli. The basal

parts of the cells showed disorganized basal infoldings and mitochondria (Figure 11b). The collecting tubular cells had rarified cytoplasm and bizarre-shaped mitochondria, and rested on a thick basement membrane (Figure 12b).

DN + ZnO-NPs group sections showed that the filtration barrier was formed of numerous thin-foot processes arising from the primary processes of podocyte, thin glomerular basement membrane and fenestrated glomerular endothelium. The glomerular capillary endothelium had heterochromatic nuclei with red blood cells in the lumen (Figure 10c). The proximal tubular cells rested on a thin regular basement membrane. They had normal cytoplasm with distinct vacuoles, lysosomes, regular euchromatic nuclei and regularly packed apical microvilli. The basal part of the cells had basal infoldings with regularly arranged mitochondria (Figure 11c). The collecting tubular cells had

Figure 8. Immune histochemical-stained sections for AQP11 cytoplasmic immune reaction (a). **a** Control group, most of the tubular cells show intense reaction. **b** DN group, some tubular cells show faint reaction. **c** DN + ZnO-NPs group, showing nearly normal reaction in the tubular cells. **d** the mean area % of positive immunoreactions in anti-aquaporin-11 immune-stained sections. Estimates are displayed as mean ± standard errors ($X \pm$ SEM); [a]: P compared to control group; [b]: P compared to DN group; [#]: $P < .05$; [##]: $P < .001$.

regular euchromatic nuclei with prominent nucleoli. They have smooth apical membrane, numerous mitochondria and also apparent vacuoles. The cells were attached to each other by a tight junction (Figure 12c).

Morphometric results

In DN group, statistical analysis revealed highly significant increases in the mean area % of collagen fiber deposition, positive PAS reactions and positive immune reactions in anti-mTOR-immune stained sections, along with the mean count of positive cells in anti-p53-stained sections, while the mean area % of positive immune reactions in anti-AQP11 sections was significantly diminished when compared to the control and DN + ZnO-NPs groups. On the other hand, ZnO-NPs treatment significantly reduced the mean area % of collagen fiber deposition, positive

PAS reactions and anti-mTOR-stained cells, and mean number of anti-p53 positive cells, and significantly enhanced mean area % of anti-AQP11-immune stained cells (Figs. 5d, 6d, 7d, 8d and 9d).

Discussion

DN is one of the most distressing complications of diabetes, and accounts for about half of the entire end-stage renal diseases worldwide. In spite of the current therapies of DN, many patients progress to develop renal failure.[2] There is an urgent need to find new therapeutic agents that could decrease disease progression, repair the impending renal damage and recover the kidney functions. Accordingly, our aim was to examine the prospective efficacy of ZnO-NPs in treating DN in streptozotocin-induced diabetic rats.
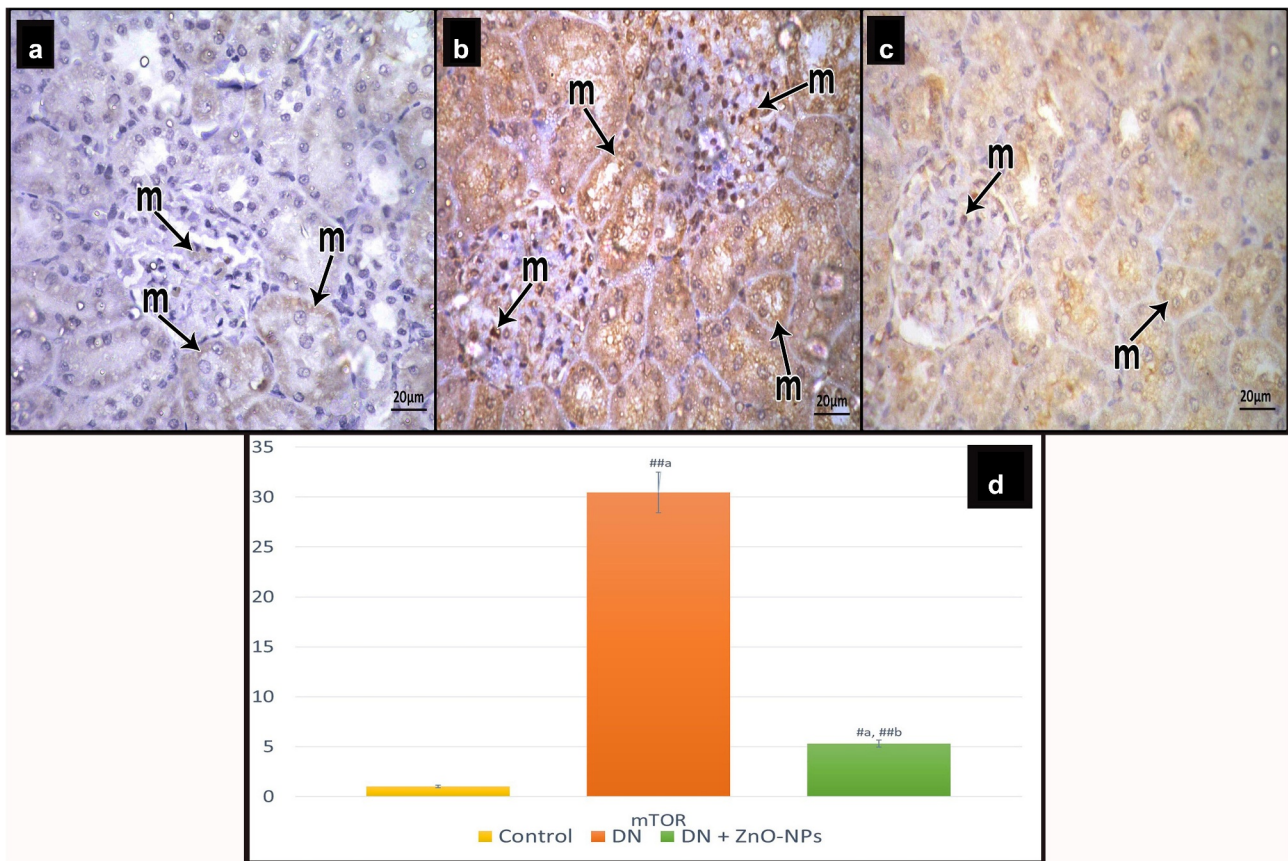
Figure 9. Immune histochemical-stained sections for mTOR showing cytoplasmic and nuclear immune reaction (m). **a** Control group, few mTOR immunoreactive cells can be detected. **b** DN group, showing increased mTOR immune reactions both in the tubular and the glomerular cells. **c** DN + ZnO-NPs group, some immune reactive cells are seen. **d** The mean area % of positive immunoreactions in anti-mTOR immune-stained sections. Estimates are displayed as mean ± standard errors (X ± SEM); [a]: P compared to control group; [b]: P compared to DN group; [#]: $P <$ .05; [##]: $P <$ .001.

In the present work, the DN group revealed impaired renal functions as indicated by the high levels of serum creatinine, BUN and proteins in urine. This was associated with altered renal structure as confirmed by light and electron microscopy examination. The fundamental changes were mesangial expansion of the glomeruli, the effacement of the podocyte foot processes and thickened basement membrane that resulted in the disrupted structure of the glomerular filtration barrier. In agreement, Chen et al.[6] reported that podocyte pathological changes affect the glomerular filtration barrier leading to proteinuria and accelerating kidney function deterioration. Hyperglycemia induces apoptosis of podocytes triggered by excessive production of reactive oxygen species (ROS).[4]

The current study recorded downregulation of mRNA expression of podocyte marker proteins; nephrin and podocin in the diabetic group. They are crucial structural proteins of the podocyte slit diaphragm that regulate the renal filtration barrier function. Podocin also facilitates the recruitment of nephrin into lipid raft microdomains of the plasma membrane at the filtration slit, which stabilizes and regulates the signaling of the glomerular filter.[35] In line with our findings, Alomari et al.[36] attributed the albumin leakage and proteinuria to the reduction of nephrin and podocin immune expression in diabetic rats. The reduction in synaptopodin, podocin and nephrin could lead to cytoskeleton abnormalities of podocyte, insufficient adhesions, and splitting between the podocyte and the glomerular basement membrane.[37] Nephrin may point to
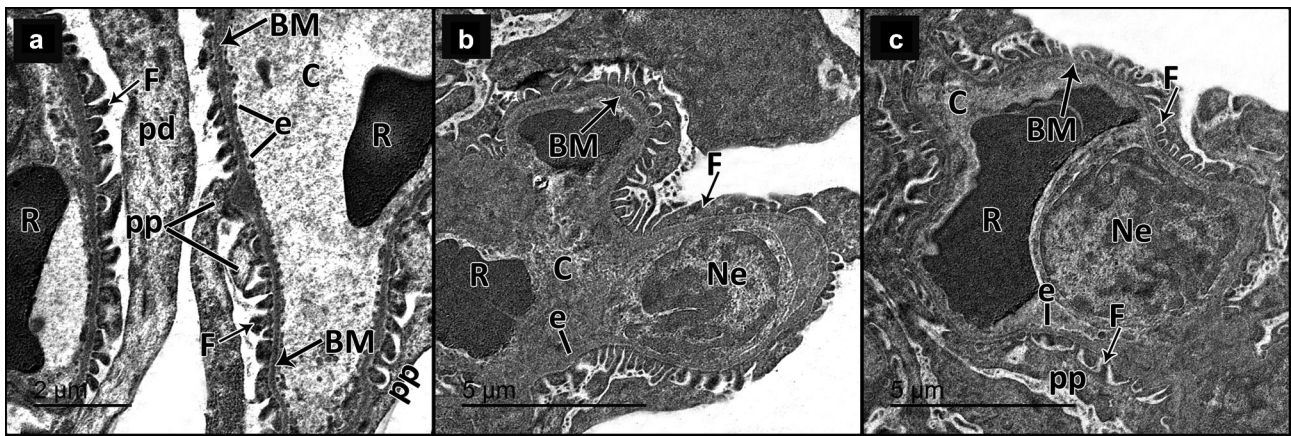
Figure 10. Electron micrographs of sections in the glomeruli of adult male rats in all study groups. **a** Control group, the glomerulus reveals part of the podocyte cell body (Pd) from which the primary processes (pp) arise. The filtration barrier is formed of many thin foot processes (f), glomerular basement membrane (BM) and fenestrated endothelium (e) of the glomerular capillaries (c). Notice red blood cells (r) in the lumen of the glomerular capillary. **b** DN group, the filtration barrier appears disturbed; the podocyte foot processes show effacement (F), some areas of the glomerular basement membrane appear thickened (BM) and the glomerular capillary (C) shows disappearance of fenestrated endothelium in some areas (e). Notice the nucleus of the endothelium (Ne). Red blood cells (R) appear in the lumen. **c** DN + ZnO-NPs group, the filtration barrier is formed of numerous thin foot processes (F) arising from the primary processes (pp) of podocyte, thin glomerular basement membrane (BM) and fenestrated glomerular endothelium (e). The glomerular capillary (C) endothelium has a heterochromatic nucleus (Ne) with red blood cells (R) in the lumen.
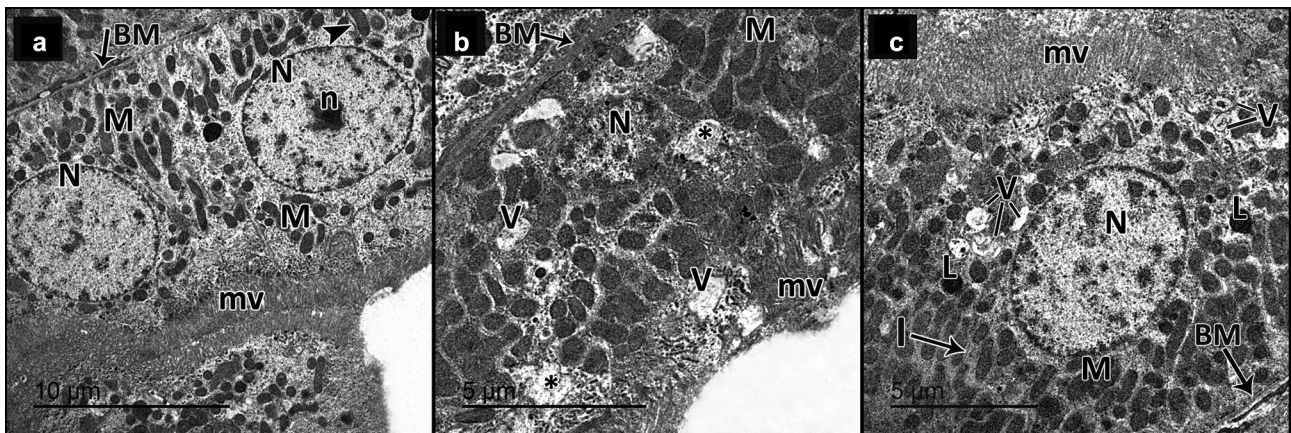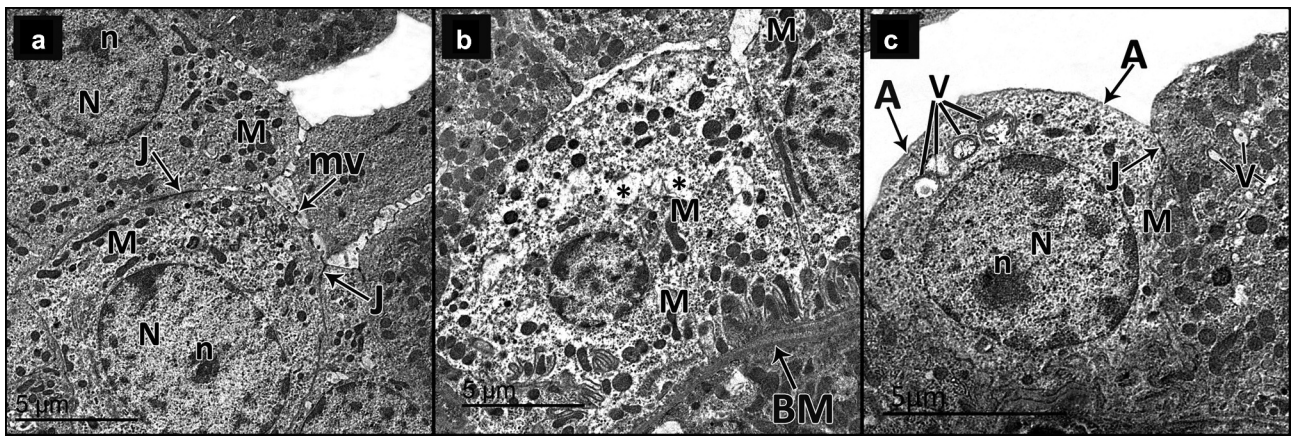

Figure 11. Electron micrographs of sections for proximal convoluted tubules of adult male rats in all study groups. **a** Control group, proximal tubular cells rest on thin regular basement membrane (BM). The tubular cells have regular euchromatic nuclei (n) with prominent nucleoli (n) and regularly packed apical microvilli (mv), the basal parts of the cells show basal infoldings (i) with regularly arranged mitochondria (m). **b** DN group, the proximal tubular cells rest on thick basement membrane (BM). They have heterochromatic nuclei (N), rarified cytoplasm (*) with some vacuolated areas (v) and disorganized apical microvilli (mv). The basal parts of the cells show disorganized basal enfolding with disorganized mitochondria (M). **c** DN + ZnO-NPs group, the proximal tubular cell rests on a thin regular basement membrane (BM). It has normal cytoplasm with evident vacuoles (V), a regular euchromatic nucleus (N), lysosomes (l) and regularly packed apical microvilli (mv). The basal part of the cell shows basal infoldings (I) with regularly arranged mitochondria (M).

early podocyte affection in diabetes; as the decreased expression of nephrin and podocin precedes the ultra-structural changes in podocytes, and the appearance of proteinuria.[38]

In the current work, structural changes in the renal tubules and blood vessels were evident in the diabetic rats. We revealed degeneration and vacuolation of the tubular cells, hyaline and cellular casts, congestion, and dilated thickened blood vessels. Our results were in agreement with Raparia e al.[39]. Gilbert[7] declared that renal tubular injury and tubulointerstitial fibrosis have a key role in the damage of the glomeruli in DN, in a process described as "diabetic tubulopathy". Inflammation

Figure 12. Electron micrographs of sections in the collecting tubule of adult male rats in all study groups. **a** Control group, the collecting tubular cells have regular euchromatic nuclei (n) with prominent nucleoli (n). They have smooth apical membrane away from few short microvilli (mv) and numerous mitochondria (m). The cells are attached to each other by tight junctions (j). **b** DN group, the collecting tubular cell has rarified cytoplasm (*) and bizarre shaped mitochondria (M) and rests on a thick basement membrane (BM). **c** DN + ZnO-NPs group, the collecting tubular cells have regular euchromatic nucleus (N) with prominent nucleoli (n). They have smooth apical membranes (a), numerous mitochondria (M) and apparent vacuoles (v). The cells are attached to each other by tight junctions (J).

of the tubular cells can affect the glomeruli and vasculature through inflammatory mediators.[40] With regard to the inflammatory process associated with diabetes, we revealed significant increases in COX-2 enzyme activity in the serum and NF-κB level in the renal tissues of the DN group, besides, the inflammatory cellular infiltration.

The diabetic group of the present study showed also significant enhancement of collagen fiber deposition around renal tubules and corpuscles, in between glomerular capillaries, and around blood vessels. Consistent with Nastase et al.[41], renal fibrosis is the usual endpoint of different chronic kidney diseases, and the degree of fibrosis determines the residual renal function. Fibrosis results from an imbalance between the formation and break down of extracellular matrix, epithelial-to-mesenchymal transition, and stimulation of fibroblasts. Hyperglycemia, oxidative stress, inflammation, ischemia, and hypoxia could be triggering factors of fibrosis.[42]

According to Takiyama and Haneda[8], hyperglycemia increases the filtration rate through the glomerular barrier and enhances sodium and glucose reabsorption in the tubular cells. So, renal tubules are vulnerable to chronic hypoxia caused by increased oxygen demand secondary to stimulation of sodium-potassium-ATPase activity in DN. In the

same context, we revealed a significant upregulation of HIF-1α in the blood of diabetic group. HIFs are stimulated by hypoxia, and can regulate different genes involved in intracellular signaling pathways.[43] HIF-1α enhances the transcription of genes that promote oxidative stress.[44] It also mediates glomerular damage by stimulating apoptosis of podocyte.[45] Moreover, HIF-1 α indorses tubulo-interstitial fibrosis via upregulation of plasminogen activator inhibitor-1.[46]

Aquaporins (AQPs), transmembrane channels, selectively transport water and some solutes across the cell. AQPs include 13 members (AQP0–AQP12), eight of them (AQP1–AQP7 and AQP11) are distributed in different parts of the kidney[47, 48]. AQP11 is mainly expressed in the proximal tubules, associated with the endoplasmic reticulum, and controlled by glucose. AQP11 plays an important role in the homeostasis of endoplasmic reticulum and in maintaining the osmolality of cytosol and vesicles. A recessive mutation in mouse AQP11 (Cysteine 227 to Serine 227) resulted in damage of the proximal tubules and renal failure in mutant animals.[11] In the present work, there was statistically significant reduction in AQP11 immune histochemical expression in the diabetic group when compared to

the controls. AQP11 inadequacy disposes to diabetic kidney disease and hyperglycemia-stimulated renal dysfunction.[49] Previously, diabetic polyuria was believed to result from osmotic diuresis due to hyperglycemia. Later, it was found that polyuria is caused by AQPs disorders.[50]

Several factors are included in the pathogenesis of DN e.g., genetic factors, hemodynamics, oxidative stress, and inflammation.[51,52] Autophagy is implicated in the pathogenesis of DN. It maintains the homeostasis of intracellular environment by degradation of proteins and peroxidases.[53] Diabetes affects podocyte autophagy through autophagy-related (Atg) protein conjugation system and mTOR regulation.[54] Induction of mTOR plays a crucial role in inhibition of pathways of autophagy.[17] According to the results of our work, the diabetic group showed an intense mTOR immune reaction in both tubular and glomerular cells. Apoptosis is also enhanced as evidenced by the significant increase in p53 immune expression. Bhang et al.[55] reported that activation of mTOR aggravates podocyte apoptosis and facilitates the advance of DN. The loss of podocytes by apoptosis impairs the glomerular filtration barrier and characterizes the early stages of DN.

By assessing the gene expression of autophagy-related proteins, we revealed downregulation of mRNA expression of proteins associated with autophagosome formation [Beclin-1 and LC3), along with enhancement of p62 mRNA expression. Our findings are consistent with the results of Liu et al.[20]. Beclin-1 expression can be used to detect the initiative stage of autophagy[56], and the conversion of LC3-I to LC3-II is considered a reliable marker for autophagosome formation.[19] Besides, p62 upregulation denotes the blockage of autophagic turnover and autolysosome maturation.[57]

Nanoparticles (NPs) have a broad range of applications in medical treatments due to their ability to pass through biological barriers and improve the bioavailability of therapeutic agents.[36] Diabetic patient commonly complains zinc deficiency due to increased urinary excretion secondary to impaired renal barrier, diminished intestinal absorption, and diet restriction.[58]

ZnO-NPs are considered unique agents for zinc delivery. They have been extensively used in biomedical and cancer therapies due to their unique physical and chemical properties.[59] The results of the current work signified that administration of ZnO-NPs recovered the renal epithelial barrier and improved the functional changes of the diabetic kidney. The treated group displayed decreased measurements of serum creatinine, BUN and proteins in urine when compared to the diabetic group. ZnO-NPs are absorbed into organs in the ionic form rather than the particulate one. The liver and kidneys are considered frequent target organs. Particles dissolve in the acidic environment of cells as they traffic from early to late endosomes then to lysosomes. The particulate component acts as a depot of zinc ions.[60] Zinc improves the barrier structure and function of the renal epithelium through its action on definite molecular targets including the proteins of tight junctional complexes.[61]

We also found that ZnO-NPs significantly decreased the blood glucose and upregulated serum insulin levels in comparison to diabetic group. This was consistent with the results of Wahba et al.,[28] who reported that ZnO-NPs exhibited antidiabetic effect by reversing pancreatic injury and increasing insulin secretion in a rat model of diabetes. As stated by Alkaladi et al.[62], ZnO-NPs could upregulate insulin gene expression. ZnO-NPs may also adjust the glucose utilization and metabolism by improving the hepatic glycogenesis.[63] Furthermore, zinc has been reported to regulate glucagon secretion from pancreatic α-cells.[64]

In the present study, ZnO-NPs treatment mostly recovered the structural and ultrastructural alterations of the kidney in a rat model of diabetic nephropathy. This was supported by the significant increase in mRNA expression of podocyte proteins (nephrin and podocin), which restored the integrity of the glomerular filtration barrier. There was also upregulation of AQP11 immune histochemical expression in the renal tubules. The area percentage of col-

lagen fibers and PAS-positive parts significantly decreased in comparison to the diabetic rats. Fernando and Zhou[58] reported decrease in collagen deposition and extracellular matrix accumulation following zinc intake in diabetic mice and concluded that zinc may play a protective role against renal injury and fibrosis in DN.

In this study, the administration of ZnO-NPs displayed highly significant decreases in the measurements of blood HIF-1α, serum COX-2 enzyme activity and tissue NF-κB, compared to the DN group. According to Nagajyothi et al.[65], ZnO-NPs demonstrated moderate antioxidant activity and powerful anti-inflammatory activity in a dose-dependent matter by inhibiting mRNA and protein expressions of inducible nitric oxide synthase (iNOS), COX-2, and inflammatory cytokines e.g., interleukin 1β, interleukin-6 and tumor necrosis factor (TNF-α). Further, Kim and Jeong[66] demonstrated that ZnO-NPs prevented the nuclear translocation of NFκB by blocking the phosphorylation and degradation of its precursors. Further, ZnO-NPs stimulated A20 expression, a zinc finger-protein and depressing regulator of NF-κB. Therefore, ZnO-NPs propose a potential way of managing inflammatory diseases.

NPs entered cells as particulate matters causing a stress reaction that induces autophagy. NPs stimulate the formation autophagosomes then degradation to autolysosomes. NPs-exposure may stimulate autophagy by inhibiting mTOR-signaling pathways[67]. In the current work, ZnO-NPs treatment significantly reduced mTOR immune reactivities in the renal glomeruli and tubules when compared to the diabetic group. In agreement with our results, Yang et al.[59] reported that ZnO nanocomposite impeded PI3K/Akt/mTOR signaling pathway, which promoted autophagy in gastric cancer cells. Inhibition of mTOR can also impede apoptosis of podocytes.[68] In accordance, we reported a significant reduction of the apoptotic marker p53 immune histochemical reactions after ZnO-NPs intake.

Our study also showed that ZnO-NPs administration promoted autophagosome synthesis, as shown by autophagic vesicles detected by electron microscopy and increased beclin-1 and LC3 mRNA expressions. ZnO-NPs also enhanced autolysosome degradation, as revealed by decreased p62 mRNA expression that also insured that the buildup of autophagosomes results from stimulated autophagy rather than suppressed autophagic flux. In line with our results, Bai et al.[69] illustrated that ZnO-NPs induced autophagy by activating LC3 protein expression. Beclin-1 expression was also enhanced following the treatment with ZnO-NPs primary peritoneal macrophages of mice[70] and titanium oxide NPs in podocytes of mice.[71]

In conclusion, administration of ZnO-NPs ameliorated the functional and histopathological alterations of the kidney in a rat model of diabetic nephropathy. ZnO-NPs retained the constancy of the glomerular filtration barrier and restored almost normal renal structure. This was confirmed by upregulation of mRNA expression of podocyte proteins (nephrin and podocin) and AQP11 immune histochemical expression in the renal tubules. The beneficial outcomes of ZnO-NPs might be attributed to activation of autophagy through inhibiting mTOR signaling pathway. ZnO-NPs promoted autophagosome synthesis followed by autolysosome degradation, as shown by enhanced beclin-1 and LC3 mRNA expressions, along with diminished p62 mRNA expression. ZnO-NPs also exerted anti apoptotic potential (evidenced by the decrease in p53 immune expression), anti-inflammatory effect (endorsed by suppression of serum COX-2 enzyme activity, and tissue NF-κB level) and anti-oxidant activity (revealed by the decrease in blood HIF-1α level). These results may point the way to an effective therapy of DN. Nevertheless, the administration to humans as a routine therapy requires many clinical trials to assess different size, doses and durations, and to avoid toxicity.

Authors' contributions

Availability of data and materials

All data generated or analyzed during this study are included in this published article.

Disclosure statement

No potential conflict of interest was reported by the author(s).

Funding

ORCID

Samia A. Abd El-Baset http://orcid.org/0000-0003-4147-3632
Nehad F. Mazen http://orcid.org/0000-0002-2942-2763
Rehab S. Abdul-Maksoud http://orcid.org/0000-0002-2241-1586
Asmaa A. A. Kattaia http://orcid.org/0000-0002-7188-0100

References

1. Souto EB, Souto SB, Campos JR, Severino P, Pashirova TN, Zakharova LY, ... Santini A. Nanoparticle delivery systems in the treatment of diabetes complications. Molecules. 2019;24(23):4209. doi:10.3390/molecules24234209.

2. Donate-Correa J, Luis-Rodríguez D, Martín-Núñez E, Tagua VG, Hernández-Carballo C, Ferri C, ... Navarro-González JF. Inflammatory targets in diabetic nephropathy. Journal of Clinical Medicine. 2020;9(2):458. doi:10.3390/jcm9020458.

3. Brosius FC, Coward RJ. Podocytes, signaling pathways, and vascular factors in diabetic kidney disease. Adv Chronic Kidney Dis. 2014;21(3):304–310. doi:10.1053/j.ackd.2014.03.011.

4. Gui D, Guo Y, Wang F, Liu W, Chen J, Chen Y, ... Wang N. Astragaloside IV, a novel antioxidant, prevents glucose-induced podocyte apoptosis in vitro and in vivo. PloS one. 2012;7(6):e39824. doi:10.1371/journal.pone.0039824.

5. Lu HJ, Tzeng TF, Liou SS, Da Lin S, Wu MC, Liu IM. Polysaccharides from liriopes radix ameliorate streptozotocin-induced type I diabetic nephropathy via regulating NF-κB and p38 MAPK signaling pathways. BMC Complement Altern Med. 2014;14(1):1–12. doi:10.1186/1472-6882-14-156.

6. Chen S, Chen H, Liu Q, Ma Q. Effect of simvastatin on the expression of nephrin, podocin, and vascular endothelial growth factor (VEGF) in podocytes of diabetic rat. Int J Clin Exp Med. 2015;8:18225.

7. Gilbert RE. Proximal tubulopathy: prime mover and key therapeutic target in diabetic kidney disease. Diabetes. 2017;66(4):791–800. doi:10.2337/db16-0796.

8. Takiyama Y, Haneda M. Hypoxia in diabetic kidneys. Biomed Res Int. 2014;2014.

9. Isoe T, Makino Y, Mizumoto K, Sakagami H, Fujita Y, Honjo J, ... Haneda M. High glucose activates HIF-1-mediated signal transduction in glomerular mesangial cells through a carbohydrate response element binding protein. Kidney Int. 2010;78(1):48–59. doi:10.1038/ki.2010.99.

10. Leung JC, Chan LY, Tsang AW, Tang SC, Lai KN. Differential expression of aquaporins in the kidneys of streptozotocin-induced diabetic mice. Nephrology. 2005;10:63–72.

11. Atochina-Vasserman EN, Biktasova A, Abramova E, Cheng DS, Polosukhin VV, Tanjore H, ... Tchekneva EE. Aquaporin 11 insufficiency modulates kidney susceptibility to oxidative stress. American Journal of Physiology-Renal Physiology. 2013;304(10):F1295–F1307. doi:10.1152/ajprenal.00344.2012.

12. Jia Z, Sun Y, Liu S, Liu Y, Yang T. COX-2 but not mPGES-1 contributes to renal PGE2 induction and diabetic proteinuria in mice with type-1 diabetes. PloS one. 2014;9(7):e93182. doi:10.1371/journal.pone.0093182.

13. Mohamed R, Jayakumar C, Ranganathan PV, Ganapathy V, Ramesh G. Kidney proximal tubular epithelial-specific overexpression of netrin-1 suppresses inflammation and albuminuria through suppression of COX-2-mediated PGE2 production in streptozotocin-induced diabetic mice. Am J Pathol. 2012;181(6):1991–2002. doi:10.1016/j.ajpath.2012.08.014.

14. Brownlee M. The pathobiology of diabetic complications: a unifying mechanism. diabetes. 2005;54(6):1615–1625. doi:10.2337/diabetes.54.6.1615.

15. Ding Y, Choi ME. Autophagy in diabetic nephropathy. J Endocrinol. 2015;224(1):R15. doi:10.1530/JOE-14-0437.

16. Xu Y, Zhou Q, Xin W, Li Z, Chen L, Wan Q. Autophagy downregulation contributes to insulin resistance mediated injury in insulin receptor knockout podocytes in vitro. PeerJ. 2016;4:e1888. doi:10.7717/peerj.1888.

17. Lin YC, Chang YH, Yang SY, Wu KD, Chu TS. Update of pathophysiology and management of diabetic kidney disease. Journal of the Formosan Medical Association. 2018;117(8):662–675. doi:10.1016/j.jfma.2018.02.007.

18. Sinha S, Levine B. The autophagy effector beclin 1: a novel BH3-only protein. Oncogene. 2008;27(S1):S137–S148. doi:10.1038/onc.2009.51.

19. Mizushima N, Yoshimori T, Levine B. Methods in mammalian autophagy research. Cell. 2010;140(3):313–326. doi:10.1016/j.cell.2010.01.028.

20. Liu WJ, Gan Y, Huang WF, Wu HL, Zhang XQ, Zheng HJ, Liu HF. Lysosome restoration to activate podocyte autophagy: a new therapeutic strategy for diabetic kidney disease. Cell Death Dis. 2019;10(11):1–17. doi:10.1038/s41419-019-2002-6.

21. Chasapis CT, Loutsidou AC, Spiliopoulou CA, Stefanidou ME. Zinc and human health: an update. Arch Toxicol. 2012;86(4):521–534. doi:10.1007/s00204-011-0775-1.

22. Jansen J, Karges W, Rink L. Zinc and diabetes—clinical links and molecular mechanisms. J Nutr Biochem. 2009;20(6):399–417. doi:10.1016/j.jnutbio.2009.01.009.

23. Chabosseau P, Rutter GA. Zinc and diabetes. Arch Biochem Biophys. 2016;611:79–85. doi:10.1016/j.abb.2016.05.022.

24. Olechnowicz J, Tinkov A, Skalny A, Suliburska J. Zinc status is associated with inflammation, oxidative stress, lipid, and glucose metabolism. The Journal of Physiological Sciences. 2018;68(1):19–31. doi:10.1007/s12576-017-0571-7.

25. Umrani RD, Paknikar KM. Zinc oxide nanoparticles show antidiabetic activity in streptozotocin-induced type 1 and 2 diabetic rats. Nanomedicine. 2014;9 (1):89–104. doi:10.2217/nnm.12.205.

26. Mosquera J, García I, Liz-Marzán LM. Cellular uptake of nanoparticles versus small molecules: a matter of size. Acc Chem Res. 2018;51(9):2305–2313. doi:10.1021/acs.accounts.8b00292.

27. Ebrahim N, Ahmed IA, Hussien NI, Dessouky AA, Farid AS, Elshazly AM, . . . Sabry D. Mesenchymal stem cell-derived exosomes ameliorated diabetic nephropathy by autophagy induction through the mTOR signaling pathway. Cells. 2018;7(12):226. doi:10.3390/cells7120226.

28. Wahba NS, Shaban SF, Kattaia AA, Kandeel SA. Efficacy of zinc oxide nanoparticles in attenuating pancreatic damage in a rat model of streptozotocin-induced diabetes. Ultrastruct Pathol. 2016;40(6):358–373. doi:10.1080/01913123.2016.1246499.

29. Ko JW, Hong ET, Lee IC, Park SH, Park JI, Seong NW, . . . Kim JC. Evaluation of 2-week repeated oral dose toxicity of 100 nm zinc oxide nanoparticles in rats. Lab Anim Res. 2015;31(3):139–147. doi:10.5625/lar.2015.31.3.139.

30. Wen L, Gao Q, Ma CW, Ge Y, You L, Liu RH, . . . Liu D. Effect of polysaccharides from Tremella fuciformis on UV-induced photoaging. J Funct Foods. 2016;20:400–410. doi:10.1016/j.jff.2015.11.014.

31. Tietz NW, Pruden EL, Fuhrman SA. Eds., Clinical guide to laboratory tests. 1995: Saunders..

32. Livak KJ, Schmittgen TD. Analysis of relative gene expression data using real-time quantitative PCR and the 2− ΔΔCT method. methods. 2001;25(4):402–408. doi:10.1006/meth.2001.1262.

33. Bancroft JD, Gamble M. Eds., 2008: Theory and practice of histological techniques.Elsevier health sciences.

34. Ayache J, Beaunier L, Boumendil J, Ehret G, Laub D. Sample preparation handbook for transmission electron microscopy techniques. New York: Springer Science and Businesss Media; 2010.

35. Verma R, Wharram B, Kovari I, Kunkel R, Nihalani D, Wary KK, . . . Holzman LB. Fyn binds to and phosphorylates the kidney slit diaphragm component nephrin. Journal of Biological Chemistry. 2003;278 (23):20716–20723. doi:10.1074/jbc.M301689200.

36. Alomari G, Al-Trad B, Hamdan S, Aljabali A, Al-Zoubi M, Bataineh N, . . . Tambuwala MM. Gold nanoparticles attenuate albuminuria by inhibiting podocyte injury in a rat model of diabetic nephropathy. Drug Deliv Transl Res. 2020;10(1):216–226. doi:10.1007/s13346-019-00675-6.

37. Eid AA, Gorin Y, Fagg BM, Maalouf R, Barnes JL, Block K, Abboud HE. Mechanisms of podocyte injury in diabetes: role of cytochrome P450 and NADPH oxidases. Diabetes. 2009;58(5):1201–1211. doi:10.2337/db08-1536.

38. Jim B, Ghanta M, Qipo A, Fan Y, Chuang PY, Cohen HW, . . . He JC. Dysregulated nephrin in diabetic nephropathy of type 2 diabetes: a cross sectional study. PloS one. 2012;7(5):e36041. doi:10.1371/journal.pone.0036041.

39. Raparia K, Usman I, Kanwar YS. Renal morphologic lesions reminiscent of diabetic nephropathy. Arch Pathol Lab Med. 2013;137(3):351–359. doi:10.5858/arpa.2012-0243-RA.

40. Baines RJ, Brunskill NJ. Tubular toxicity of proteinuria. Nat Rev Nephrol. 2011;7(3):177–180. doi:10.1038/nrneph.2010.174.

41. Nastase MV, Zeng-Brouwers J, Wygrecka M, Schaefer L. Targeting renal fibrosis: mechanisms and drug delivery systems. Adv Drug Deliv Rev. 2018;129:295–307. doi:10.1016/j.addr.2017.12.019.

42. Melmed S, Polonsky KS, Larsen PR, Kronenberg HM. Williams textbook of endocrinology E-Book. Elsevier Health Sciences.2015 ;.

43. Nangaku M, Inagi R, Miyata T, Fujita T. Hypoxia and hypoxia-inducible factor in renal disease. Nephron Exp Nephrol. 2008;110(1):e1–e7. doi:10.1159/000148256.

44. Diebold I, Petry A, Hess J, Görlach A. The NADPH oxidase subunit NOX4 is a new target gene of the hypoxia-inducible factor-1. Mol Biol Cell. 2010;21 (12):2087–2096. doi:10.1091/mbc.e09-12-1003.

45. Brukamp K, Jim B, Moeller MJ, Haase VH. Hypoxia and podocyte-specific vhlh deletion confer risk of glomerular disease. American Journal of Physiology-Renal Physiology. 2007;293(4):F1397–F1407. doi:10.1152/ajprenal.00133.2007.

46. Higgins DF, Kimura K, Bernhardt WM, Shrimanker N, Akai Y, Hohenstein B, Saito Y, Johnson RS, Kretzler M, Cohen CD, et al. Hypoxia promotes fibrogenesis in vivo via HIF-1 stimulation of epithelial-to-mesenchymal transition. J Clin Invest. 2007;117(12):3810–3820. doi:10.1172/JCI30487.

47. Li Y, Wang W, Jiang T, Yang B. Aquaporins in urinary system. Aquaporins. 2017;131–148.

48. Soveral G, Casini A. Aquaporin modulators: a patent review. Expert Opin Ther Pat. 2010–2015 2017;27(1):49–62. doi:10.1080/13543776.2017.1236085.

49. Choma DP, Vanacore R, Naylor H, Zimmerman IA, Pavlichenko A, Pavlichenko A, Foye L, Carbone DP, Harris RC, Dikov MM, et al. Aquaporin 11 variant associates with kidney disease in type 2 diabetic patients. American Journal of Physiology-Renal Physiology. 2016;310(5):F416–F425. doi:10.1152/ajprenal.00295.2015.

50. Shafaei H, Rad JS, Behjati M, Behjati M. The effect of pulp and seed extract of citrullus colocynthis, as an antidaibetic medicinal herb, on hepatocytes glycogen stores in diabetic rabbits. Advanced Biomedical Research. 2014 Advanced biomedical research, 3.3;258:(1). doi:10.4103/2277-9175.148230.

51. Forbes JM, Fukami K, Cooper ME. Diabetic nephropathy: where hemodynamics meets metabolism. Experimental and Clinical Endocrinology & Diabetes. 2007;115(2):69–84. doi:10.1055/s-2007-949721.

52. Kanwar YS, Wada J, Sun L, Xie P, Wallner EI, Chen S, . . . Danesh FR. Diabetic nephropathy: mechanisms of renal disease progression. Exp Biol Med. 2008;233(1):4–11. doi:10.3181/0705-MR-134.

53. Kim WY, Nam SA, Song HC, Ko JS, Park SH, Kim HL, . . . Kim YK. The role of autophagy in unilateral ureteral obstruction rat model. Nephrology. 2012;17(2):148–159. doi:10.1111/j.1440-1797.2011.01541.x.

54. Zhu J, Wang KZ, Chu CT. After the banquet: mitochondrial biogenesis, mitophagy, and cell survival. Autophagy. 2013;9(11):1663–1676. doi:10.4161/auto.24135.

55. Bhang SH, Lee S, Shin JY, Lee TJ, Jang HK, Kim BS. Efficacious and clinically relevant conditioned medium of human adipose-derived stem cells for therapeutic angiogenesis. Molecular Therapy. 2014;22(4):862–872. doi:10.1038/mt.2013.301.

56. Wang X, Sun D, Hu Y, Xu X, Jiang W, Shang H, Cui D. The roles of oxidative stress and Beclin-1 in the autophagosome clearance impairment triggered by cardiac arrest. Free Radic Biol Med. 2019;136:87–95. doi:10.1016/j.freeradbiomed.2018.12.039.

57. Guo C, Yang M, Jing LI, Wang J, Yu Y, Li Y, . . . Sun Z. Amorphous silica nanoparticles trigger vascular endothelial cell injury through apoptosis and autophagy via reactive oxygen species-mediated MAPK/Bcl-2 and PI3K/Akt/mTOR signaling. Int J Nanomedicine. 2016;11:5257.

58. Fernando J, Zhou S. The role of zinc in renal pathological changes in diabetic status.2015 ..

59. Yang Z, Pu M, Dong X, Ji F, Veeraraghavan VP, Yang H. Piperine loaded zinc oxide nanocomposite inhibits the PI3K/AKT/mTOR signaling pathway via attenuating the development of gastric carcinoma: in vitro and in vivo studies. Arabian Journal of Chemistry. 2020;13(5):5501–5516. doi:10.1016/j.arabjc.2020.03.028.

60. Baek M, Chung H-E, Yu J, Lee J-A, Kim T-H, Oh J-M, Lee W-J, Paek S-M, Lee JK, Jeong J. Pharmacokinetics, tissue distribution, and excretion of zinc oxide nanoparticles. Int J Nanomedicine. 2012;7:3081. doi:10.2147/IJN.S32593.

61. Wang X, Valenzano MC, Mercado JM, Zurbach EP, Flounders CJ, Mullin JM. Zinc enhancement of LLC-PK(1) renal epithelial barrier function. Clinical Nutrition (Edinburgh, Scotland). 2014;33(2):280–286. Clinical nutrition. doi:10.1016/j.clnu.2013.05.001.

62. Alkaladi A, Abdelazim AM, Afifi M. Antidiabetic activity of zinc oxide and silver nanoparticles on streptozotocin-induced diabetic rats. Int J Mol Sci. 2014;15(2):2015–2023. doi:10.3390/ijms15022015.

63. Quesada I, Tudurí E, Ripoll C, Nadal A. Physiology of the pancreatic α-cell and glucagon secretion: role in glucose homeostasis and diabetes. Journal of Endocrinology. 2008;199(1):5–19. doi:10.1677/JOE-08-0290.

64. Egefjord L, Petersen AB, Bak AM, Rungby J. Zinc, alpha cells and glucagon secretion. Curr Diabetes Rev. 2010;6(1):52–57. doi:10.2174/157339910790442655.

65. Nagajyothi PC, Cha SJ, Yang IJ, Sreekanth TVM, Kim KJ, Shin HM. Antioxidant and anti-inflammatory activities of zinc oxide nanoparticles synthesized using Polygala tenuifolia root extract. J Photochem Photobiol B. 2015;146:10–17. doi:10.1016/j.jphotobiol.2015.02.008.

66. Kim MH, Jeong HJ. Zinc oxide nanoparticles suppress LPS-induced NF-κB activation by Inducing A20, a negative regulator of NF-κB, in RAW 264.7 macrophages. J Nanosci Nanotechnol. 2015;15(9):6509–6515. doi:10.1166/jnn.2015.10319.

67. Jia L, Hao SL, Yang WX. Nanoparticles induce autophagy via mTOR pathway inhibition and reactive oxygen species generation. Nanomedicine. 2020;15(14):1419–1435. doi:10.2217/nnm-2019-0387.

68. Xue R, Zhai R, Xie L, Zheng Z, Jian G, Chen T, Gui D. Xuesaitong protects podocytes from apoptosis in diabetic rats through modulating PTEN-PDK1-Akt-mTOR pathway. J Diabetes Res. 2020;2020:1–12. doi:10.1155/2020/9309768.

69. Bai DP, Zhang XF, Zhang GL, Huang YF, Gurunathan S. Zinc oxide nanoparticles induce apoptosis and autophagy in human ovarian cancer cells. Int J Nanomedicine. 2017;12:6521. doi:10.2147/IJN.S140071.

70. Zhang X, Yin H, Li Z, Zhang T, Yang Z. Nano-TiO 2 induces autophagy to protect against cell death through antioxidative mechanism in podocytes. Cell Biol Toxicol. 2016;32(6):513–527. doi:10.1007/s10565-016-9352-y.

71. Roy R, Singh SK, Chauhan LKS, Das M, Tripathi A, Dwivedi PD. Zinc oxide nanoparticles induce apoptosis by enhancement of autophagy via PI3K/Akt/mTOR inhibition. Toxicol Lett. 2014;227(1):29–40. doi:10.1016/j.toxlet.2014.02.024.